Strategies for Ambiguity Resolution in LEO-PNT Systems with Various Frequency Bands

Massarweh, Lotfi; Verhagen, Sandra

DOI
10.1109/PLANS61210.2025.11028483

Publication date
2025

Document Version
Final published version

Published in
2025 IEEE/ION Position, Location and Navigation Symposium, PLANS 2025

Strategies for Ambiguity Resolution in LEO-PNT Systems with Various Frequency Bands

Lotfi Massarweh
Geoscience and Remote Sensing
Delft University of Technology
Delft, The Netherlands
L.Massarweh@tudelft.nl
ORCID: 0000-0003-0320-7413

Sandra Verhagen
Geoscience and Remote Sensing
Delft University of Technology
Delft, The Netherlands
Sandra.Verhagen@tudelft.nl
ORCID: 0000-0002-4107-2364

2025 IEEE/ION Position, Location and Navigation Symposium (PLANS) | 979-8-3315-2317-6/25/$31.00 ©2025 IEEE | DOI: 10.1109/PLANS61210.2025.11028483

***Abstract*—In this paper, we investigate strategies for ambiguity resolution in Low Earth Orbit Positioning, Navigation, and Timing (LEO-PNT) systems, particularly across multiple frequency bands beyond the traditional L-band used in GNSS. By leveraging the rapid geometric change of LEO satellites, our study examines the feasibility of fast and reliable integer ambiguity resolution (IAR) in Precise Point Positioning with Ambiguity Resolution (PPP-AR). Using end-to-end simulations, we assess the impact of different signal bands on convergence time and positioning accuracy. The methodology incorporates the LAMBDA 4.0 toolbox for mixed-integer estimation models, providing insights into how LEO-PNT enhances PPP-AR performance. Results demonstrate significant improvements in ambiguity resolution success rates and positioning convergence when incorporating LEO signals, highlighting their potential in future PNT application.**

***Index Terms*—Global Navigation Satellite System, LEO-PNT, Precise Point Positioning, Ambiguity Resolution, LAMBDA.**

I. Introduction

The advent of low Earth orbit positioning, navigation, and timing (LEO-PNT) systems is expected to revolutionize precise positioning services by offering improved signal strength, reduced multipath effects and resilience to interference, along with an enhanced coverage over challenging environments such as polar regions and urban canyons. Compared to traditional Global Navigation Satellite Systems (GNSS), LEO-PNT satellites benefit from their rapid geometric change, which accelerates the convergence time for the ground user position coordinates. Additionally, novel signals/frequency bands are planned to be demonstrated [1], thus extending the capabilities of current L-band signals to other frequency bands.

A successful resolution of the unknown integer ambiguities in carrier-phase measurements is a critical component for achieving centimeter-level positioning accuracy with short times-to-fix, i.e. fundamental for Precise Point Positioning with Ambiguity Resolution (PPP-AR), see [2]. This Integer Ambiguity Resolution (IAR) process depends on multiple factors, including the wavelength of the tracked signal and the precision of code/phase observations. Although alternative higher frequency bands, for example, the S or C bands, offer potential advantages [3], including a reduced ionospheric delay and lower multipath-induced code errors, shorter wavelengths associated with higher frequencies introduce challenges for ambiguity resolution, potentially necessitating novel IAR approaches.

In this work, we discuss IAR strategies for future LEO-PNT systems, particularly for signals beyond the commonly used L-band. The study evaluates the feasibility of ambiguity resolution using end-to-end numerical simulations, examining different scenarios and signal configurations. An uncombined and undifferenced formulation of the PPP-AR user model is adopted, but assuming no errors in the provision of real-time corrections from a ground (regional) network estimation. The ambiguities are decorrelated and integer-estimated using the recently developed Least-squares AMBiguity Decorrelation Adjustment (LAMBDA) 4.0 toolbox [4]. The LAMBDA approach works with a linear combination of carrier-phase ambiguities, accounting for their correlation among different constellations, satellites, and signals. In this way, we show how successful ambiguity resolution can be carried out for LEO-PNT systems, with instantaneous convergence enabled by the rapid changes of satellite geometry. This study does not evaluate the impact of the uncertainty in the estimated satellite corrections, which remains a fundamental aspect for IAR, but is dependent on the network estimation strategy (to be) defined by future LEO-PNT service providers.

In Section II, we briefly review LEO-PNT systems, considering existing and planned constellations, then we define the uncombined and undifferenced formulation in use for PPP-AR, focusing on the user model. In Section III, we describe the methodology of the end-to-end numerical simulations, including the main assumptions and models adopted. In Section IV, we present the numerical results considering a representative LEO-PNT constellation for all analyses. We evaluated the kinematic positioning performance in terms of convergence time and investigated the challenges of ambiguity resolution with respect to different frequency bands. Lastly, in Section V, we provide a summary and recommendations for future work.

II. Literature Review

A. LEO-PNT constellations

The current trend of mega-constellations in low Earth orbit (LEO) was originally driven by communication satellites. In

TABLE I
OVERVIEW OF DEDICATED LEO-PNT SYSTEMS WITH NUMBER OF SATELLITES AND FREQUENCY BANDS (AS OF DECEMBER 2024), SEE [1].

Constellation	Country	#Sats	Altitude [km]	Bands	Status
STL/Iridium Communications	US	66	780	L	Deployed
PULSAR/Xona Space Systems	US	258	∼1000	L	On-going
TrustPoint	US	288	500–800 (TBD)	C	On-going
GeeSAT/GeeSpace	CN	240	620	L	On-going
CENTISPACE/Future Navigation	CN	190	975–1100	L	On-going
LEO-PNT/European Space Agency	EU	up to 263	550 (IOD)	UHF/L/S/C	Planned
ArkEdge Space & JAXA	JP	(TBD)	(TBD)	VHF/C	Feasibility
Skykraft Pty Ltd	AU/IN	(TBD)	(TBD)	S	Feasibility

early 2015, multiple applications were submitted for the spectrum allocation of large LEO constellations [5], with additional systems later proposed for broadband applications. In these last ten years, the number of active satellites in LEO has grown from less than 1400 to over 10000, with OneWeb consisting of around 660 satellites and SpaceX's Starlink network currently operating almost 7000 satellites (for a total of 12000 recently approved by the United States' Federal Communications Commission). However, these megaconstellations are not dedicated to Positioning-Navigation-Timing (PNT) applications [6], and the use of so-called signals of opportunity (SOP) from such non-PNT systems has been largely studied; see [7], [8].

When looking at dedicated LEO-PNT systems, one of the first commercial augmentation services is the Iridium Communications' Satellite Time and Location (STL) service, operative since May 2016 and providing a resilient PNT solution via Iridium 66-satellite constellation [9]. Additional LEO-based systems (see Table I) have been designed and are currently being deployed:

- Xona's PULSAR constellation [10]: first technology demonstrator satellite launched on 25 May 2022, and with around 258 satellites planned at around 1000 km.
- TrustPoint constellation [11]: first cubesat-based satellite launched on 15 April 2023, and around 288 satellites planned for global coverage focusing on C-band services.
- GeeSpace's GeeSAT constellation [12]: inaugural launch on 2 June 2022 and a total of 240 satellites expected at around 620 km.
- Future Navigation's CENTISPACE constellation [13]: first launch on 29 September 2018 (at 700 km), designed for a total of 190 satellites in three layers:
  - 120 satellites at 975 km (55.0° inclination)
  - 30 satellites at 1100 km (87.4° inclination)
  - 40 satellites at 1100 km (30.0° inclination)

along with the planned

- LEO-PNT in-orbit demonstrator (IOD) mission to be deployed by the European Space Agency (ESA), thus consisting of two parallel contracts, led by GMV Innovating Solutions (12U CubeSat) and Thales Alenia Space (16U CubeSat), respectively. These Pathfinder A satellites will be followed in 2027 by two mini-constellations of four Microsats (Pathfinder B) in quasi-polar orbits (∼ 550 km) and transmitting on different frequency bands [14].

Furthermore, ArkEdge Space has initiated feasibility studies in collaboration with the Japan Aerospace Exploration Agency (JAXA), and Skykraft via a partnership agreement among Australian and Indian organizations [7].

Although most of these new systems foresee to transmit L-band signals, other alternative frequency bands have been studied as well [15], with potential use of S-band (e.g., 2483.5–2500 MHz) and C-band (e.g., 5010–5030 MHz). The former one is already in use by the Globalstar 48-satellite constellation for the Augmented Positioning System (APS), which is a non-dedicated PNT service complementary to GPS.

B. Uncombined/Undifferenced PPP-AR model

We start considering the observation equations

$$\begin{aligned} \mathrm{E}\{p^s_{r,j}\} &= \rho^s_r + dt^s_r + d^s_{r,j} + m^s_r\tau_r + \mu_j \imath^s_{r,1} \\ \mathrm{E}\{\phi^s_{r,j}\} &= \rho^s_r + dt^s_r + \delta^s_{r,j} + m^s_r\tau_r - \mu_j \imath^s_{r,1} + \lambda_j N^s_{r,j} \end{aligned} \tag{1}$$

where $p^s_{r,j}$ are the code and $\phi^s_{r,j}$ the phase observations, with $\mathrm{E}\{\cdot\}$ referring to the expectation operator. For the user receiver r tracking a satellite s on the j-th signal frequency f_j, the geometric range is ρ^s_r, $dt^s_r = dt_r - dt^s$ is the receiver-minus-satellite clock offset, and $d^s_{r,j} = d_{r,j} - d^s_{,j}$ and $\delta^s_{r,j} = \delta_{r,j} - \delta^s_{,j}$ refer to code and phase hardware delays, respectively. The troposphere slant delay is modeled as $m^s_r\tau_r$ given a troposphere mapping function m^s_r and a wet delay τ_r. Dispersive atmospheric delays are also present, caused by the ionosphere contribution referred, in a first-order approximation, to the first frequency, i.e. $\imath^s_{r,1}$, and then multiplied by the ionospheric coefficient $\mu_j = f_1^2/f_j^2$.

The carrier-phase ambiguities are defined by $N^s_{r,j} \in \mathbb{Z}$. They comprise of the unknown integer number of cycles with wavelength $\lambda_j = c/f_j$ for $c = 299792458\ m/s$ (speed of light in vacuum), plus the initial phase offsets. For signals in the L-band (1-2 GHz), we have wavelengths of 15-30 cm, but the current GNSS signals generally vary between 19 and 26 cm. The S-band (2-4 GHz) and C-band (4-8 GHz) signals have wavelengths of 7.5-15 cm and 3.75-7.5 cm, respectively, therefore having very short wavelengths that might be challenging for a successful ambiguity resolution.

Following the linearization given an initial user position, we can correct the code and phase observations based on

$$\mathrm{E}\left\{\begin{pmatrix}\Delta p_{r,1}\\ \Delta p_{r,2}\\ \Delta p_{r,3}\\ \Delta \phi_{r,1}\\ \Delta \phi_{r,2}\\ \Delta \phi_{r,3}\end{pmatrix}\right\} = \begin{bmatrix} G_r & u_m & & & & +\mu_1 I_m & & & \\ G_r & u_m & & & & +\mu_2 I_m & & & \\ G_r & u_m & u_m & & & +\mu_3 I_m & & & \\ G_r & u_m & & u_m & & -\mu_1 I_m & \lambda_1 C_m & & \\ G_r & u_m & & & u_m & -\mu_2 I_m & & \lambda_2 C_m & \\ G_r & u_m & & & & u_m & -\mu_3 I_m & & & \lambda_3 C_m \end{bmatrix} \begin{pmatrix}\delta x_r\\ \tilde{dt}_r\\ \tilde{d}_{r,3}\\ \tilde{\delta}_{r,1}\\ \tilde{\delta}_{r,2}\\ \tilde{\delta}_{r,3}\\ \tilde{i}_{r,1}\\ \tilde{N}^s_{r,1}\\ \tilde{N}^s_{r,2}\\ \tilde{N}^s_{r,3}\end{pmatrix} \tag{2}$$

deterministic models and apply satellite corrections to obtain the observed-minus-computed observations, i.e. $p^s_{r,j} \rightarrow \Delta p^s_{r,j}$ and $\phi^s_{r,j} \rightarrow \Delta \phi^s_{r,j}$. For a single-GNSS constellation, we define the triple-frequency PPP-AR user model in (2), where the user coordinate (East-North-Up) displacements and the Zenith Wet Delay (ZWD) are both included in the parameter vector δx_r. The estimable ambiguities $\tilde{N}^s_{r,1}$ are of a double-differenced nature, see eq.(3), and therefore integer-valued since the initial phase offsets are canceled out.

The tilde notation '$\sim$' refers to estimable user parameters, with the following interpretation:

$$\begin{aligned} \tilde{dt}_r &= dt_{r1} + d_{r1,\mathrm{IF}} \\ \tilde{\delta}_{r,j} &= \delta_{r1,j} - [d_{r1,\mathrm{IF}} - \mu_j d_{r1,\mathrm{GF}}] + N^p_{r1,j} \\ \tilde{i}^s_{r,1} &= i^s_{r,1} + [d_{r,\mathrm{GF}} - d^s_{,\mathrm{GF}}] \\ \tilde{N}^s_{r,1} &= N^s_{r1,j} - N^p_{r1,j} \end{aligned} \tag{3}$$

and an additional estimable receiver code bias is defined by

$$\tilde{d}_{r,[j>2]} = d_{r1,[j>2]} - (d_{r1,\mathrm{IF}} + \mu_{[j>2]} d_{r1,\mathrm{GF}}) \tag{4}$$

where '$(\cdot)_{r1}$' refers to '$(\cdot)_r - (\cdot)_1$' as the difference between the user receiver and a certain *pivot* receiver adopted in the network estimation of satellite corrections, which is absorbed by the user parametrization. The notation 'IF' and 'GF' respectively refer to ionosphere-free and geometry-free combinations based on two reference signals [17], given as follows

$$\xi_{,\mathrm{GF}} = \frac{\xi_{,2} - \xi_{,1}}{\mu_2 - \mu_1}, \quad \xi_{,\mathrm{IF}} = \frac{\mu_2 \xi_{,1} - \mu_1 \xi_{,2}}{\mu_2 - \mu_1} \tag{5}$$

The following auxiliary quantities have been used:

- u_m as m-dimensional vector of 1s,
- I_m as $m \times m$ identity matrix,
- C_m as $m \times (m-1)$ matrix constructed from I_m, thus removing the p-th column associated to the pivot satellite, e.g. the highest elevation satellite (per each system).

The stochastic model for the observables assumes no correlation between code and phase data, along with no correlation between signal frequencies. The observable errors are assumed to be zero-mean and normally distributed with a certain standard deviation, e.g. $\sigma_p/\sigma_\phi = 30cm/3mm$ for code/phase data, respectively. In kinematic positioning, we assume user receiver coordinates and the clock offset, as well as slant ionospheric delays to be unlinked in time. However, a small process noise for the ZWD can be considered. The code-phase biases and ambiguities are assumed to be constant in time.

For multi-constellation scenarios, we define an inter-system bias (ISB) that refers to the difference of time offsets (between constellations), and it also accounts for the differences in receiver delays that might arise even for overlapping frequencies. We refer to [19], [20] for more information. In this contribution, we consider LEO-PNT systems as *external* constellation not synchronized with the reference one, e.g. GPS or Galileo, so estimating an ISB as a constant term.

C. Mixed-integer models

The linear system in (2) can be more simply generalized by a mixed-integer model [21]:

$$\mathrm{E}\{y\} = Aa + Bb, \quad \mathrm{D}\{y\} = Q_{yy} \in \mathbb{R}^{m \times m} \tag{6}$$

where $\mathrm{D}\{\cdot\}$ is the dispersion operator, and the vector $y \in \mathbb{R}^m$ contains code and phase observables again assumed to be normally distributed, i.e. $y \sim \mathcal{N}_m(Aa + Bb, Q_{yy})$, with the variance-covariance matrix $Q_{yy} \in \mathbb{R}^{m \times m}$ being positive definite. The full-rank design matrix $[A, B] \in \mathbb{R}^{m \times (n+p)}$ defines the functional relation with the estimable unknowns, thus referring here to integer ambiguities $a \in \mathbb{R}^n$ and real-valued parameters $b \in \mathbb{R}^p$.

The least-squares solution follows by a *primal* orthogonal decomposition [22], where we consider

$$||y - Aa - Bb||^2_{Q_{yy}} = \|\hat{e}\|^2_{Q_{yy}} + \|\hat{a} - a\|^2_{Q_{\hat{a}\hat{a}}} + \left\|\hat{b}(a) - b\right\|^2_{Q_{\hat{b}(a)}} \tag{7}$$

where $\|x\|^2_Q = x^T Q^{-1} x$ is the weighted squared norm of vector x under the metric defined by matrix Q. The least-squares residuals' vector is $\hat{e} \in \mathbb{R}^m$, where no constraints are accounted for in the estimation. Therefore, the three-step approach [23], can be adopted:

1) **Float solution**. The integerness of ambiguities is discarded and we compute the float estimators $\hat{a} \in \mathbb{R}^n$ and $\hat{b} \in \mathbb{R}^p$ via a standard least-squares solution;

2) **Ambiguity resolution**. A fixed ambiguity estimator $\breve{a} = \mathcal{I}_a(\hat{a})$ is obtained by a mapping function $\mathcal{I}_a : \mathbb{R}^n \to \mathbb{Z}^n$;

3) **Fixed solution**. We conditionally update the real-valued parameters on the fixed ambiguities, i.e. $\breve{b} = \hat{b}(\breve{a})$.

with no constraints set for the real-valued parameters, therefore the ambiguity-fixed solution will directly be given by $\hat{b}(z)$ for an integer vector $z \in \mathbb{Z}^n$.

An efficient implementation to search integer ambiguities is available by means of the recently released **LAMBDA 4.0 toolbox**, see [4], which considers $\hat{a}$ and $Q_{\hat{a}\hat{a}}$ as inputs. In the LAMBDA method [22] three different classes of estimators are available, as illustrated in Fig.1, with each one characterized by different properties based on the family of maps $\mathcal{I}_a$ being defined. A decorrelation step takes place by means of a linear combination of ambiguities to be considered for the integer ambiguity resolution (Step 2).

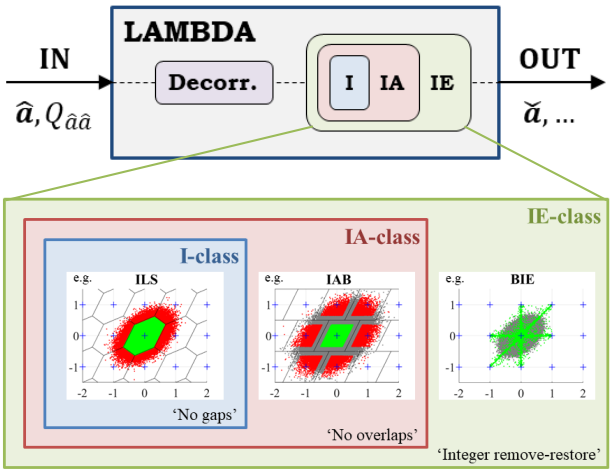

Fig. 1. Flowchart of LAMBDA 4.0 toolbox with its three classes of estimators (I = integer, IA = integer aperture, IE = integer equivariant), as described in the LAMBDA Documentation [4]

III. Methodology

We use the TU Delft's LEO-enhanced Positioning with Ambiguity Resolution Demonstrator (LEOPARD) platform [24], [25] for carrying out end-to-end simulations. Two main modules are configured: with the space segment module we define the GNSS and/or LEO-PNT constellations including the satellite orbits, clocks, and other design parameters (e.g. signal frequencies); the user segment module allows us defining user position and clock, along with biases estimated in a sequential Kalman Filter (KF) approach.

In Fig.2, a simplified flow chart is presented, where the PPP-AR estimation module (integrating LAMBDA 4.0 toolbox) is visible. The user ambiguity-float and ambiguity-fixed solutions are then used in the analysis tool for generating the principal statistical metrics in the performance evaluation, such as the convergence time.

In the measurements' generation and PPP-AR solution's estimation we account for several real-world physical delays on the signal propagation, such as relativistic effects (excluding J_2 contributions), atmospheric dispersive and non-dispersive delays, site displacements (solid Earth tides, ocean tides), according to the International Earth Rotation Service (IERS) 2010 conventions [26]. An overview of models/assumptions is given in Table II, where we differentiate between the 'generation' and 'estimation' steps.

We account for

- **Troposphere:** the hydrostatic tropospheric slant delay is accurately modeled in the estimation, while we account for the wet troposphere delay based on the Global Pressure Temperature 2 wet (GPT2w) empirical model[1] developed by [27]. A residual ZWD parameter is estimated as a random walk with small process noise, e.g. 6 $mm/\sqrt{h}$, see [28].
- **Ionosphere:** the generated slant atmospheric dispersive delay is based on the assumption of a single-layer vertical distribution of total electron content (TEC) with spherical harmonics (up to 5×5 degrees) located at 450 km. The vertical-to-slant mapping assumes a thin layer, while slant TEC values are estimated based on an ionosphere-float model [17], i.e., biased by a linear combination of code biases.

In the estimation part, ocean tides are neglected with small errors ~ 1 cm found in the positioning solution, i.e., mainly in the vertical component. The receiver clock offset and inter-system biases are respectively generated using a random walk (with large process noise) and as constant values (over 1 day), whereas clocks are then assumed unlinked in time in the KF estimation. The latter is initialized by a least-squares solution with a Gauss-Newton iterative algorithm that tackles the non-linearity in position coordinates, with an initial position defined tens of kilometers away from the true user location. An elevation mask of 7° is adopted, assuming open-sky scenarios with static REDU user that is processed in a kinematic solution, i.e. based on an epoch-wise estimation of receiver coordinates and clocks.

Real-world phenomena such as multipath effects or cycle-slip events are not considered in this contribution, also because these are highly dependent on the LEO-PNT receiver configuration and tracking capability [3]. Furthermore, we also neglect the uncertainty of satellite products, which depend on the network estimation strategy (and receiver distribution) set by the correction provider. These aspects will be investigated in future works.

IV. Numerical Results

Here we provide the numerical results, where we mainly look at the convergence time for different configurations.

[1] Available online at https://vmf.geo.tuwien.ac.at/products.html

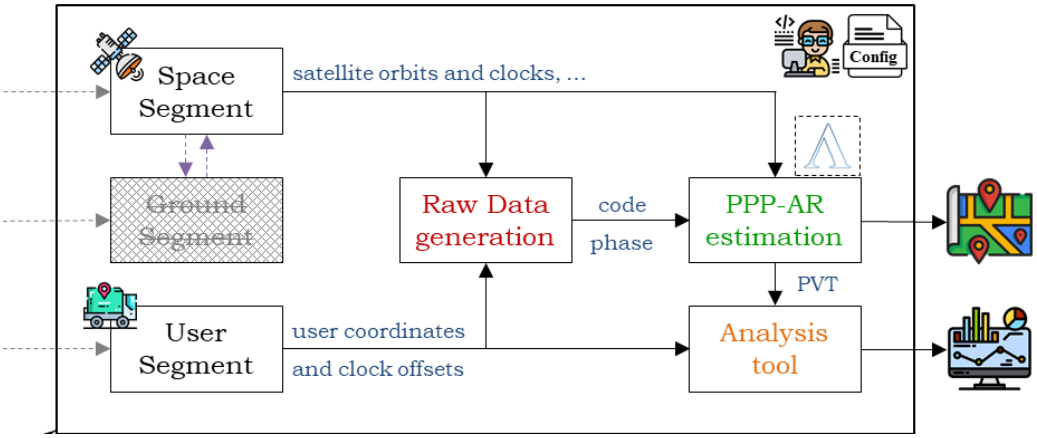

Fig. 2. Top-level architecture of the LEOPARD simulation environment [24], [25] used in this study

TABLE II
STRATEGIES FOR THE MEASUREMENT GENERATION (RDG) AND SOLUTION ESTIMATION (PPP-AR).

Variable	Generation (RDG)	Estimation (PPP-AR)
Observables' type	Code & Phase	Code & Phase
Observables' noise	Gaussian, zero-mean	Kalman Filter
Receiver clock offset	Random walk (large process noise)	Estimated per epoch
Inter-System Bias	Constant (over 1 day)	Estimated as constant
Ionospheric effects	Single layer (at 450 km)	Estimated per epoch (iono-float)
Troposphere effects	Hydrostatic + Wet delays (GPT2w)	ZHD modeled, ZWD estimated
Solid Earth Tides	Modeled (IERS 2010)	Modeled (IERS 2010)
Ocean Tides	Modeled (IERS 2010)	Neglected ($\sim 1\ cm$ error)
Travel time, relativistic effects, phase wind up, ...	Modeled	Modeled

We consider a nominal 24-satellite GPS-only dual-frequency (L1+L2) scenario as baseline for the analyses, referring to the REDU00BEL station receiver (approx. 50° latitude, 5° longitude, 370 m elevation). The LEO-PNT constellation is a fictitious 30-satellite constellation at 975 km altitude, with six orbital planes at 55° inclination. As such, it represents a subset of the CentiSpace system (layer #1), which ensures around 1-2 LEO satellites always in view (see Fig.3).

We start with GPS (L1+L2) and LEO (E1+E5a) configuration, thus comparing in Fig.4 the kinematic positioning errors for ambiguity-float (blue) and ambiguity-fixed (red) solutions, which are reset every 2 hours over a 12-hour period. The dashed blue lines refer to the 3σ (formal) standard deviation of the estimated coordinates. The fixed solutions of the GPS + LEO case immediately converge, where a partial ambiguity resolution (PAR) approach has been considered with a minimum success rate of 99 5%.

When looking into the IAR results in Fig.5, we observe how for the GPS-only case we have an increasing number of fixed ambiguities in time (in red) since the success rate of fixing the full set approaches 100% after around 10-20 minutes. On the other hand, for the GPS+LEO configuration we see that the success rate gradually increases, never reaching 100%. Still, nearly all integer ambiguities can be fixed. This apparently counterintuitive result has a simple explanation: the

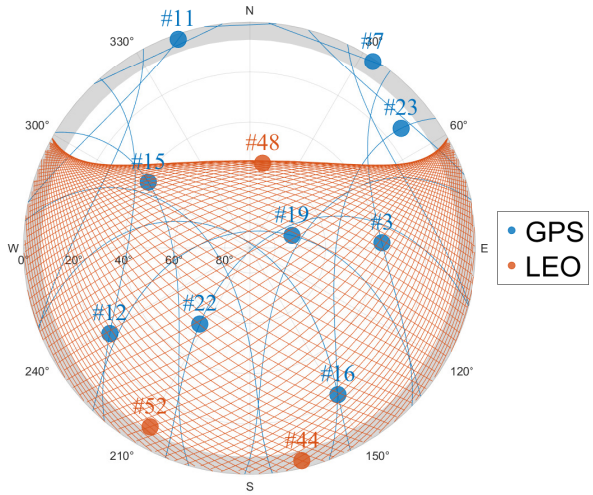

Fig. 3. Skyplot over 12 hours for GPS+LEO (24+30 satellites) combination with respect to REDU ground station.

continuous rising and setting of one or two LEO satellites introduces new ambiguities, which decreases the probability of correctly fixing $a \in \mathbb{Z}^n$ for the full set of ambiguities. By excluding the least precise (decorrelated) ambiguity, we obtain an almost instantaneous 100% success rate as visible in the

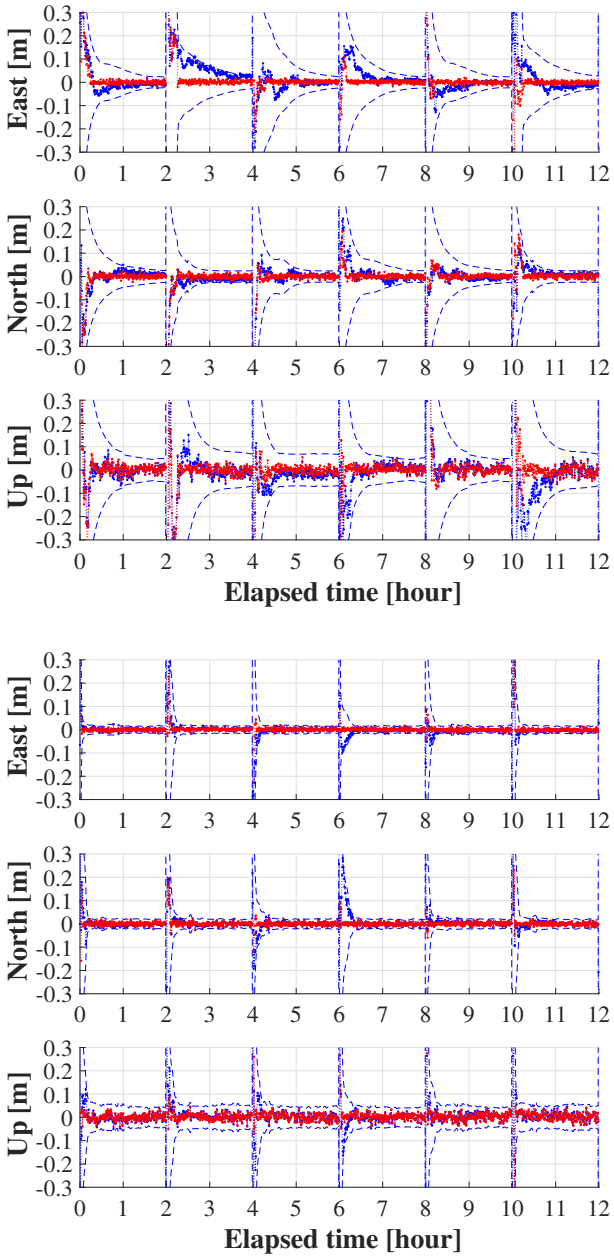

Fig. 4. Time series of positioning errors over 12 hours with 2-hour reset, showing both float (blue) and fixed (red) solutions for the GPS-only (top panel) and GPS+LEO (bottom panel) dual-frequency case.

fourth panel of Fig.5, with only small drops when a second LEO satellite is in view. This confirms that a PAR approach (following LAMBDA decorrelation of ambiguities) is highly beneficial for kinematic PPP-AR users.

The previous results are further confirmed by an analysis of the convergence time, where we consider 1-hour windows shifted by five minutes over 24 hours and compute the 90-percentile (P90) of errors for both *float* and *fixed* solutions. The results are shown in Fig.6, where we look at the East-North-Up (ENU) coordinates for GPS-only (left) and GPS+LEO

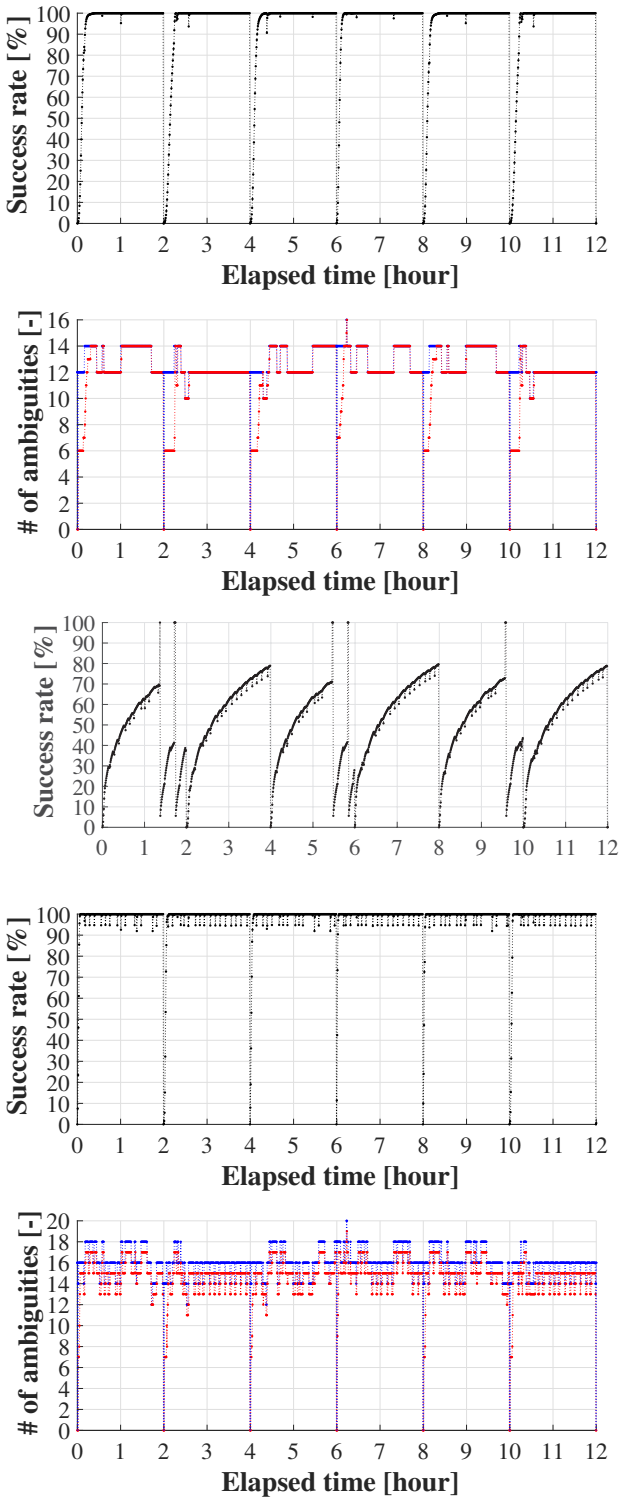

Fig. 5. Time series of ambiguity resolution performance over 12 hours with 2-hour reset, showing success rates of full-set AR and the number of float (blue) and fixed (red) ambiguities. Top (2) panels: dual-frequency GPS-only; Bottom (3) panels: dual-frequency GPS+LEO where success rates are shown with full-set AR and in case least precise ambiguity is neglected, i.e., after LAMBDA decorrelation step.

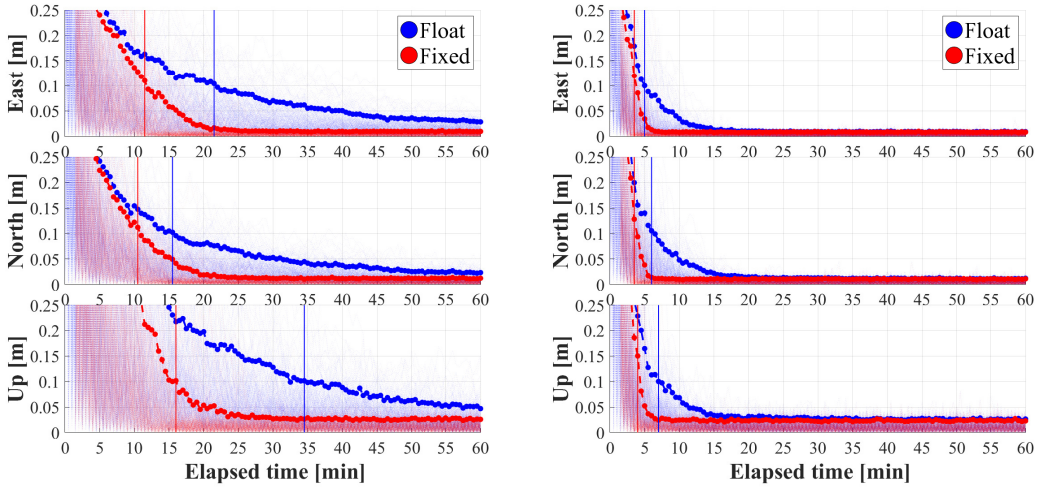

Fig. 6. Comparison of East-North-Up (ENU) coordinates' convergence for GPS-only (left) and GPS+LEO (right), see text for details.

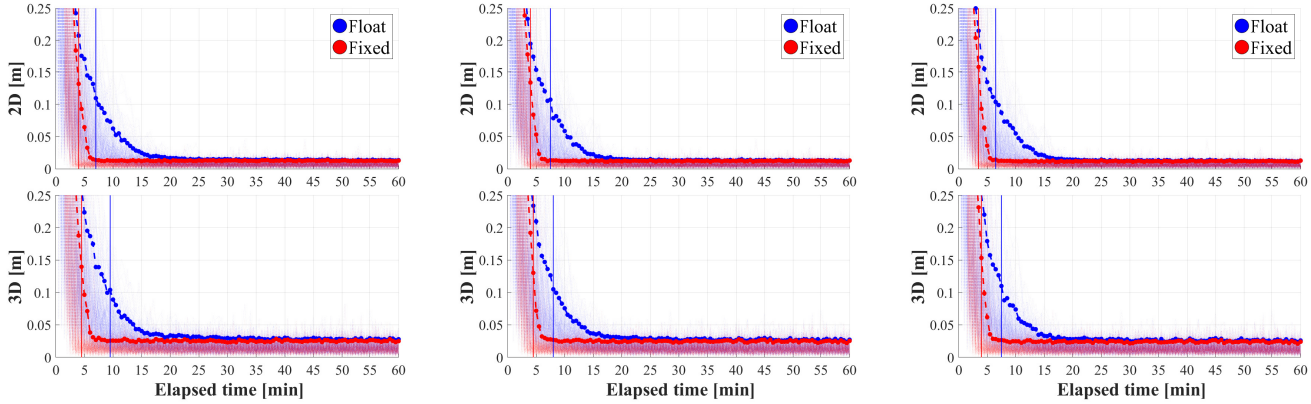

Fig. 7. Comparison of 2D/3D convergence time for GPS+LEO, where the latter makes use of L-band (L5), S-band (2500 MHz), and C-band (5020 MHz) frequency signals in addition to L1.

(right). A significant improvement on the convergence time is found, with ambiguity-fixed solutions converging in a few minutes due to the LEO satellite augmentation. In fact, the rapid geometric change largely enhanced the float solution, thus also benefiting the IAR process.

Therefore, the LEO-enhanced float solution seems to outperform even the GPS-only fixed solution, where only 1-2 satellites in view are able to drastically reduce the convergence time. Based on a partial ambiguity resolution, it is observed how a success rate close to 1 is achieve instantaneously thanks to the rapid geometry changes introduced by the LEO satellites (while keeping L-band signals in the processing).

A. Beyond L-band frequencies

At this point we consider other frequency bands for the LEO satellites, namely the S-band and C-band signals using 2500 MHz and 5020 MHz as reference frequencies, respectively. The results are presented in Fig.7, where we compare the L-band (left), S-band (center), and C-band (right) convergence results for the 2D (horizontal) and 3D positioning error components. Also in this case, both float and fixed solutions are shown in blue and red, respectively.

Surprisingly we observe little variations in the kinematic PPP/PPP-AR convergence performance among the different frequency scenarios. While at higher frequencies we have smaller wavelengths, we should mention that the rapid change of geometry acts similarly on the three cases for the float solution (i.e. neglecting the integerness of carrier-phase ambiguities). Moreover, when looking at ambiguity-fixed performance, the PAR strategy adopted in this study also has a beneficial impact since removes those less precise (decorrelated) ambiguities to maintain a success rate relatively close to 1.

With a sufficient number of phase ambiguities resolved within minutes, the convergence can be achieved in a few minutes, while it is not really affected by the choice of signal frequency for the 1-2 LEO satellites in view. This last consideration is a possible consequence of the uncombined/undifferenced formulation adopted here for PPP-AR,

along with LAMBDA capabilities to resolve ambiguities without relying on specific combinations (e.g. wide-lane or narrow-lane ambiguities). In fact, in the latter case, the adoption of higher signal frequencies could highly affect the user's capability of successfully fixing the ambiguities, especially when no decorrelation step is adopted.

V. Conclusions

In this work we focus on low Earth orbit (LEO) constellations for positioning, navigation, and timing (PNT) applications. In recent years, the interest for dedicated LEO-PNT systems has grown exponentially, with several large constellations planned to be deployed for global coverage. Most of these systems will serve as an augmentation to existing Global Navigation Satellite System (GNSS) constellations, with anticipated benefits in terms of reduced multipath effects and convergence time, along with greater resilience to interference due to an improved signal strength.

Different orbital designs and configurations are considered for these constellations, where the potential adoption of signal frequencies outside the L-band is also under discussion. The close vicinity of LEO satellites to ground users enables the usage of S-band or C-band signals, with expected reduced ionospheric delays and multipath effects. However, shorter wavelengths can pose a challenge for ambiguity resolution, which is still fundamental in order to fully exploit the millimeter-level precision of phase data. Once (a sufficiently large subset of) ambiguities are successfully resolved, improved kinematic positioning performance can be observed, especially during the filter convergence. This is numerically evaluated in this work using TU Delft's LEO-enhanced Positioning w/ Ambiguity Resolution Demonstrator (LEOPARD) platform, which integrates the LAMBDA 4.0 toolbox.

The results of this study underscore the substantial benefits that LEO-PNT systems offer for precise positioning and ambiguity resolution. The simulations reveal that the introduction of LEO signals significantly enhances the ambiguity resolution process, reducing convergence times, and improving the success rates of fixed solutions. Rapid geometric change of LEO satellites enables near instantaneous resolution of a sufficiently large set of integer ambiguities in kinematic scenarios, outperforming conventional GNSS-only PPP-AR methods. Additionally, our analysis suggests that alternative frequency bands, such as the S-band and C-band, offer similar performance in terms of convergence time for a constellation with only a few satellites in view. It should be further investigated how the performance is affected in case more LEO satellites and fewer GNSS/MEO satellites are in view.

Future research should focus on the integration of multi-constellation LEO-PNT networks and their impact on global positioning accuracy, along with the robustness of LEO-PNT solutions under real-world conditions, including multipath effects and corrections' uncertainties. Ultimately, the development of optimized filtering techniques for satellite corrections will play a crucial role in fully achieving the potential of LEO-PNT services in real-time navigation applications.

References

[1] Eissfeller, Bernd, Pany, Thomas, Dötterböck, Dominik, Förstner, Roger, "A Comparative Study of LEO-PNT Systems and Concepts," Proceedings of the ION 2024 Pacific PNT Meeting, Honolulu, Hawaii, April 2024, pp. 758-782. https://doi.org/10.33012/2024.19646

[2] Teunissen, P.J.G. (2020). GNSS Precise Point Positioning. In Position, Navigation, and Timing Technologies in the 21st Century (eds Y.T.J. Morton, F. Diggelen, J.J. Spilker, B.W. Parkinson, S. Lo and G. Gao). https://doi.org/10.1002/9781119458449.ch20

[3] De Bast, S., Sleewaegen, J.-M., and De Wilde, W. (2023). Analysis of Multipath Code-Range Errors in Future LEO-PNT Systems. Engineering Proceedings, 54(1), 34. https://doi.org/10.3390/ENC2023-15453

[4] Massarweh, L., Verhagen, S. and Teunissen, P.J.G. New LAMBDA toolbox for mixed-integer models: estimation and evaluation. GPS Solut 29, 14 (2025). https://doi.org/10.1007/s10291-024-01738-z

[5] Reid, T. G. R., Neish, A. M., Walter, T., and Enge, P. K. (2018) Broadband LEO Constellations for Navigation. J Inst Navig, 65: 205–220. https://doi.org/10.1002/navi.234.

[6] F. S. Prol et al., "Position, Navigation, and Timing (PNT) Through Low Earth Orbit (LEO) Satellites: A Survey on Current Status, Challenges, and Opportunities," in IEEE Access, vol. 10, pp. 83971-84002, 2022, doi: 10.1109/ACCESS.2022.3194050.

[7] FrontierSI (2025) State of the market report: LEO-PNT, 2024 edition. Available at https://frontiersi.com.au/wp-content/uploads/2025/01/FrontierSI-State-of-Market-Report-LEO-PNT-2024-Edition.pdf, accessed: 2025-02-01

[8] NAVAC (2024) White Paper on PNT Vision 2035. Available at https://navisp.esa.int/uploads/files/documents/NAVAC%20White%20Paper%20May%202024.pdf, accessed: 2025-02-01

[9] Hockenberry D (2016) Iridium launches breakthrough alternative GPS service. Available at https://investor.iridium.com/may-23-2016, iridium Investor Relations: Press Release May 23, 2016, accessed: 2025-02-01

[10] Christina Youn (2023) Xona Space Systems. In: International Committee on Global Navigation Satellite Systems (ICG) Workshop on Low Earth Orbit (LEO) Positioning Navigation and Timing (PNT) Systems, 9 June 2023, Vienna International Centre, Vienna.

[11] Paul Anderson (2023) TrustPoint System/Service Overview. In: International Committee on Global Navigation Satellite Systems (ICG) Workshop on Low Earth Orbit (LEO) Positioning Navigation and Timing (PNT) Systems, 9 June 2023, Vienna International Centre, Vienna.

[12] GeeSpace, "GeeSpace launches nine satellites," Geely News, 2022. Available online at: https://www.geely.com/en/news/2022/geespace-launches-nine-satellites.

[13] Xucheng Mu (2023) CENTISPACE LEO Augmentation Navigation System Status. In: International Committee on Global Navigation Satellite Systems (ICG) Workshop on Low Earth Orbit (LEO) Positioning Navigation and Timing (PNT) Systems, 9 June 2023, Vienna International Centre, Vienna.

[14] Falcone M (2024) ESA shaping the future of navigation. In: 11th ESA Workshop on Satellite Navigation Technologies (NAVITEC) 2024, ESA/ESTEC, Noordwijk, The Netherlands, presented at the 11th ESA Workshop on Satellite Navigation Technologies (NAVITEC) 2024.

[15] Wang, K., Zhang, S., and Wang, J. (2020). Feasibility of using an S-band GNSS carrier by comparing with L and C bands. Advances in Space Research, 66(9), 2232-2244.

[16] Li, X., Barriot, JP., Lou, Y. et al. Towards Millimeter-Level Accuracy in GNSS-Based Space Geodesy: A Review of Error Budget for GNSS Precise Point Positioning. Surv Geophys 44, 1691–1780 (2023). https://doi.org/10.1007/s10712-023-09785-w

[17] Zhang, B., Hou, P., Zha, J. et al. PPP–RTK functional models formulated with undifferenced and uncombined GNSS observations. Satell Navig 3, 3 (2022). https://doi.org/10.1186/s43020-022-00064-4

[18] Wu, Z., Lu, C., Tan, Y. et al. Real-time GNSS tropospheric delay estimation with a novel global random walk processing noise model (GRM). J Geod 97, 112 (2023). https://doi.org/10.1007/s00190-023-01780-8

[19] Khodabandeh, A., Teunissen, P.J.G. PPP-RTK and inter-system biases: the ISB look-up table as a means to support multi-system PPP-RTK. J Geod 90, 837–851 (2016). https://doi.org/10.1007/s00190-016-0914-9

[20] Odijk, D., Nadarajah, N., Zaminpardaz, S. et al. GPS, Galileo, QZSS and IRNSS differential ISBs: estimation and application. GPS Solut 21, 439–450 (2017). https://doi.org/10.1007/s10291-016-0536-y

[21] Massarweh L (2025) Primal and dual mixed-integer models for global navigation satellite systems. PhD thesis, Delft University of Technology, DOI 10.4233/uuid:54c03c6e-5a2e-448b-9f6a-869d673cd4dc
[22] Teunissen PJG (1993) Least-squares estimation of the integer GPS ambiguities. In: Invited lecture, section IV theory and methodology, IAG general meeting, Beijing, China, pp 1–16
[23] Teunissen, P.J.G. The least-squares ambiguity decorrelation adjustment: a method for fast GPS integer ambiguity estimation. Journal of Geodesy 70, 65–82 (1995). https://doi.org/10.1007/BF00863419
[24] Massarweh L (2024a) Numerical assessment of LEO-PNT performance: a comparison between ambiguity-float and ambiguity-fixed precise point positioning solutions. In: Proceedings of the European Navigation Conference (ENC) 2024, ESA/ESTEC, Noordwijk, The Netherlands, presented at the European Navigation Conference (ENC) 2024, 22–24 May.
[25] Massarweh L (2024b) Impact of modelling errors on LEO-PNT performance: a brief numerical investigation on ambiguity-fixed positioning. In: 11th ESA Workshop on Satellite Navigation Technologies (NAVITEC) 2024, ESA/ESTEC, Noordwijk, The Netherlands, presented at the 11th ESA Workshop on Satellite Navigation Technologies (NAVITEC) 2024.
[26] Petit G, Luzum B (2010) Iers conventions (2010). Tech. Rep. IERS Technical Note 36, International Earth Rotation and Reference Systems Service (IERS), Frankfurt am Main, Germany, 179 pp.
[27] Böhm, J., Möller, G., Schindelegger, M. et al. Development of an improved empirical model for slant delays in the troposphere (GPT2w). GPS Solut 19, 433–441 (2015). https://doi.org/10.1007/s10291-014-0403-7
[28] Young, Z.M., Blewitt, G. and Kreemer, C. Improved GPS tropospheric path delay estimation using variable random walk process noise. J Geod 98, 89 (2024). https://doi.org/10.1007/s00190-024-01898-3